ACS APPLIED ENGINEERING MATERIALS

pubs.acs.org/acsaenm Article

Alkali-Metal-Modified Al-PMOF for Enhanced CO_2 Adsorption and Photocatalytic Reduction

Chenyue Yong, Guanhong Lu, Xiao Wang, Gansheng Shi, Yan Wang, Xiaofeng Xie, and Jing Sun*

Cite This: https://doi.org/10.1021/acsaenm.5c00076 Read Online

ACCESS | Metrics & More | Article Recommendations | Supporting Information

ABSTRACT: In this paper, M-Al-PMOF (M = Na, K) composites were synthesized for the first time by incorporating alkali metals into Al-PMOFs. Comprehensive experiments were conducted to investigate the CO_2 adsorption and photocatalytic reduction capabilities of the synthesized composites with different doping amounts and types of alkali metals. The results show that doping alkali metals into Al-PMOFs efficiently enhanced their CO_2 adsorption by increasing the surface area and alkaline sites. Moreover, the modified materials exhibit improved light absorption, reduced band gap, and suppressed recombination of photogenerated electron−hole pairs, leading to a significantly enhanced photocatalytic CO_2-to-CO conversion efficiency. Notably, the 1-K-Al-PMOF sample showed a 45% increase in CO_2 adsorption capacity compared to that of pristine Al-PMOF, along with a 6.6 times enhancement in the CO production yield. This work reveals that different amounts and types of doped alkali metals can improve their CO_2 absorption and photocatalytic reduction properties, offering a perspective for designing and modifying MOFs.

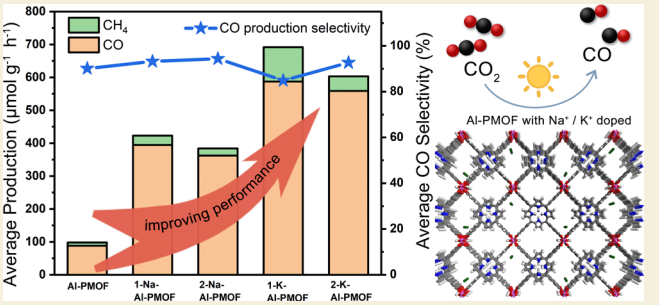

KEYWORDS: *metal−organic framework, Al-PMOF, alkali metals, CO_2 adsorption, photocatalytic CO_2 reduction*

Downloaded via SHANGHAI INST OF CERAMICS on May 18, 2025 at 13:10:02 (UTC).
See https://pubs.acs.org/sharingguidelines for options on how to legitimately share published articles.

1. INTRODUCTION

With the rapid increase in fossil fuel consumption, greenhouse gases have led to climate change and threaten human survival.[1,2] Among these greenhouse gases, carbon dioxide (CO_2) accounts for approximately 26% of the total, and its concentration continues to rise sharply. Consequently, controlling CO_2 emissions has become a global challenge. In addition, CO_2, as a carbon resource, can be reduced to high-value C1 chemicals through photocatalysis.[3,4] However, traditional CO_2 capture and utilization technologies are complex and energy-intensive, involving multiple intermediate steps, such as CO_2 capture, adsorbent regeneration, CO_2 compression, and transportation.[5] Therefore, from the perspectives of green chemistry and sustainable development, developing photocatalysts that can efficiently capture and convert CO_2 into value-added products is a promising way to address future CO_2 emissions.

Metal−organic frameworks (MOFs) have demonstrated excellent applications in catalysis and gas storage due to their advantages, such as unsaturated metal coordination, ease of surface modification, and high capacity for CO_2 adsorption.[6] Therefore, they are highly promising materials for the adsorption and catalytic reduction of the adsorption of CO_2. Among the methods used to further modify and enhance MOFs, metal metathesis stands as an effective strategy to achieve improved properties.[7,8] In particular, recent research studies suggest that incorporating alkali metals into MOFs can enhance their gas storage capacity and change local charge density inside MOFs.[9−11] For instance, Akbari Beni and Niknam Shahrak[12] discovered that lithium-functionalized ZIF-8 and ZIF-90 could significantly enhance CO_2 uptake by up to 7 and 9 times, respectively, through density functional theory (DFT) and Grand Canonical Monte Carlo (GCMC) simulations. Cui et al.[13] synthesized M-Mg/DOBDC (M = Li, Na, K) composites by doping alkali metals into Mg/DOBDC MOF and found that 0.5K-Mg/DOBDC exhibits a CO_2 adsorption capacity of 14.93 mmol g^{-1}, which was 3.44 times higher than that of Mg/DOBDC. However, most of the research studies are only focused on theoretical frameworks and computer modeling, and the understanding of how alkali metal doping in MOFs influences photocatalytic CO_2 reduction remains largely unexplored.

Therefore, in this work, we comprehensively investigated the impact of doping alkali metal ions (Na^+, K^+) into MOFs on their CO_2 adsorption and photocatalytic reduction capabilities. Among the diverse available MOFs, aluminum-based porphyrinic metal−organic framework (Al-PMOF) was selected for its

Received: January 31, 2025
Revised: April 18, 2025
Accepted: May 8, 2025

© XXXX American Chemical Society

potential in CO_2 capture and photocatalytic reduction.[14−16] Because of its simple preparation and easy doping, Al-PMOF is ideal for studying the effect of alkali metal ion doping. To our knowledge, we are the first to modify Al-PMOF by doping it with different alkali metals (Na, K) to enhance its performance both as a CO_2 absorbent and a reductive photocatalyst. Experimental results reveal that 1-K-Al-PMOF increased the CO_2 adsorption capacity by 45% compared to that of Al-PMOF. Furthermore, the doped MOFs exhibit enhanced photocatalytic CO_2-to-CO conversion efficiencies, achieving CO production increased by over 6 times with 1-K-Al-PMOF. This work offers a molecular-level perspective for designing and modifying MOFs by improving their CO_2 absorption and photocatalytic reduction properties through alkali metal doping.

2. MATERIALS AND METHODS

2.1. Chemicals and Reagents

Aluminum nitrate nonahydrate ($Al(NO_3)_3{\cdot}9H_2O$, ≥98%), 5,10,15,20-tetrakis(4-carboxyphenyl) porphyrin ($C_{48}H_{30}N_4O_8$, H_2TCPP, 95%), sodium chloride (NaCl, ≥99.9%), potassium chloride (KCl, ≥99.9%), and *N*,*N*-dimethylformamide (C_3H_7NO, DMF, ≥99.5%) were purchased from Shanghai Titan Technology Co., Ltd. All chemicals and reagents were used as received without further purification.

2.2. Synthesis Process

2.2.1. Synthesis of Aluminum-Based Porphyrinic Metal−Organic Framework (Al-PMOF). Al-PMOF was synthesized via a typical hydrothermal method.[17] 100 mg of $Al(NO_3)_3{\cdot}9H_2O$ (0.25 mmol) was added to 10 mL of deionized water and stirred. 100 mg of H_2TCPP (0.126 mmol) was added to 10 mL of deionized water and stirred. The above solution was then mixed to get the Al precursor solution and transferred to a 100 mL Teflon-lined stainless-steel autoclave with 10 min of stirring and 5 min of ultrasonication. The autoclave was then heated at 180 °C for 24 h. After being cooled to room temperature, the reactant was washed several times with deionized water, DMF, and acetone and then dried in a vacuum oven at 60 °C overnight. The obtained powder was collected and denoted as Al-PMOF.

2.2.2. Synthesis of Alkali Metal (Na, K)-Doped Aluminum-Based Porphyrinic Metal−Organic Framework (M-Al-PMOF (M = Na, K)). The synthesis of M-Al-PMOF (M = Na, K) followed a procedure similar to that of Al-PMOF, with the exception of incorporating different amounts of NaCl or KCl into the Al precursor solution. Specifically, 0.25 or 0.5 mmol of NaCl or KCl was added and dissolved in the Al precursor solution. After the hydrothermal reaction and postprocessing as described, the product was denoted as M-Al-PMOF (M = Na, K). In particular, Al-PMOF with 0.25 mmol of NaCl was denoted as 1-Na-Al-PMOF, and Al-PMOF with 0.5 mmol of NaCl was denoted as 2-Na-Al-PMOF. Similarly, Al-PMOF with 0.25 mmol of KCl was denoted as 1-K-Al-PMOF, and Al-PMOF with 0.5 mmol of KCl was denoted as 2-K-Al-PMOF.

2.3. Characterization

Scanning electron microscopy (SEM) analysis was carried out using a field emission scanning electron microscope (FEI Magellan 400) operated at an accelerating voltage of 15 kV. Powder X-ray diffraction (XRD) patterns were collected using a Bruker D8 ADVANCE instrument with Cu Kα radiation (λ = 0.15418 nm) at room temperature. The scanning range was set to 10−60°, and the scanning speed was set to 2° min^{-1}. Fourier transform infrared (FTIR) spectroscopy was conducted by using a Thermo Fisher Scientific Nicolet iN10 spectrometer. All samples were prepared using the potassium bromide (KBr) tableting method (the mass ratio of the sample to KBr was 1:100), and the scanning range was set to 500−4000 cm^{-1}. Thermogravimetric analysis (TGA) was conducted by a thermogravimetric analyzer (Netzsch STA 449 F3, Germany). Inductively coupled plasma optical emission spectroscopy (ICP-OES) was collected by an Optima 8000, PerkinElmer instrument. The Brunauer−Emmett−Teller (BET) specific surface area analysis and CO_2 adsorption isotherms of the materials were tested using a specific surface area and pore size analyzer (JW-BK100, JWGB Instruments). The in situ FTIR spectra of the samples were obtained using a Thermo Fisher iN10 iZ10 Infrared Spectrophotometer. UV−vis diffuse reflectance spectroscopy (UV−vis DRS) measurements were performed on a LAMBDA 1050+ spectrophotometer (PerkinElmer). The wavelength range was set to 200−800 nm, with $BaSO_4$ as a reference. The photoluminescence (PL) spectra were measured by using a fluorescent spectrophotometer (LS55 spectrometer, PerkinElmer Instruments). Carbon dioxide temperature-programmed desorption (CO_2-TPD) analysis was performed by a chemical temperature-programmed adsorption analyzer (ChemiSorb PCA-1200, Bibuilder, China).

2.4. Electrochemical Measurements

Electrochemical impedance spectroscopy (EIS) tests and Mott−Schottky tests were recorded in a CHI650B electrochemical workstation (Shanghai, China) with a standard three-electrode system. A fluorine-doped tin-oxide conductive glass (FTO, 25 × 15 mm^2) coated with catalyst ink was used as the working electrode. Ag/AgCl and platinum plate were used as the reference electrode and counter electrode, respectively, and a 0.3 M Na_2SO_4 (99.7%, Titan) aqueous solution served as the electrolyte (E vs RHE = E vs Ag/AgCl + 0.0591 pH + 0.197, pH = 7). Alternating current voltage was set to 1.50 V, and the test frequency range was set to 1−10^5 Hz. Transient photocurrent response (TPR) measurements were conducted using the same three-electrode system as EIS tests, with additional 250 W xenon lamp irradiation (7ILX150A, SOFN INSTRUMENTS CO., Ltd.).

2.5. Photocatalytic Performance Measurements

Photocatalytic CO_2 reduction experiments were conducted using an Agilent 7890B gas chromatograph (GC) under 500 W xenon lamp (CEL-WLAX500, 300−2500 nm, CHINA EDUCATION AU-LIGHT Co., Ltd., Beijing) irradiation, and schematic diagrams of the reaction device are shown in Figure S1. Typically, 10 mg of the prepared photocatalyst was uniformly dispersed in a 400 mL Pyrex reactor containing 10 mL of a mixed solution of deionized water, acetonitrile (C_2H_3N, ACN, ≥99.6%, Titan), and triethanolamine ($C_6H_{15}NO_3$, TEOA, ≥99%, Titan) in a volume ratio of 8:2:1 (catalyst concentration of 1 g L^{-1}). Before irradiation, CO_2 was continuously bubbled into the reactor under dark conditions to completely remove dissolved gases and ensure CO_2 saturation. During irradiation, the reaction temperature was maintained at 20 °C by using a circulating water system. The control experiments were performed without the catalyst, in darkness, and with CO_2 replaced by Ar gas.

The selectivity of photocatalytic CO_2 conversion to CO was calculated according to the following eq 1:[18]

$$\text{CO selectivity (\%)} = \frac{\text{Number of produced CO molecules}}{\text{Number of produced CO molecules and } CH_4 \text{ molecules}} \times 100\% \quad (1)$$

2.6. DFT Calculation Methods

Spin-polarized DFT calculations were performed using the Vienna Ab initio Simulation Package (VASP).[19] An electron exchange−correlation effect was handled by the Perdew−Burke−Ernzerhof (PBE) functional of the generalized gradient approximation (GGA). The DFT-D3 methodology with Becke-Johnson damping function was used to describe the dispersion interactions.[20,21] All structural models were optimized with a plane-wave expansion energy cutoff of 550 eV. The periodic cluster model structure of M-Al-PMOF was placed inside a box of 40 × 40 × 30 Å, and the K-points were set to 1 × 1 × 1. The energy convergence criterion was set to be 10^{-5} eV. All structures were fully relaxed until the residual forces on each atom

https://doi.org/10.1021/acsaenm.5c00076
ACS Appl. Eng. Mater. XXXX, XXX, XXX−XXX

Scheme 1. Schematic Diagram of the Synthetic Process of M-Al-PMOF (M = Na, K)

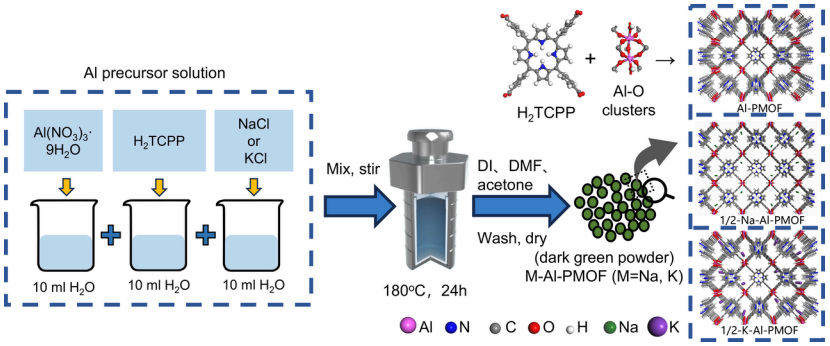

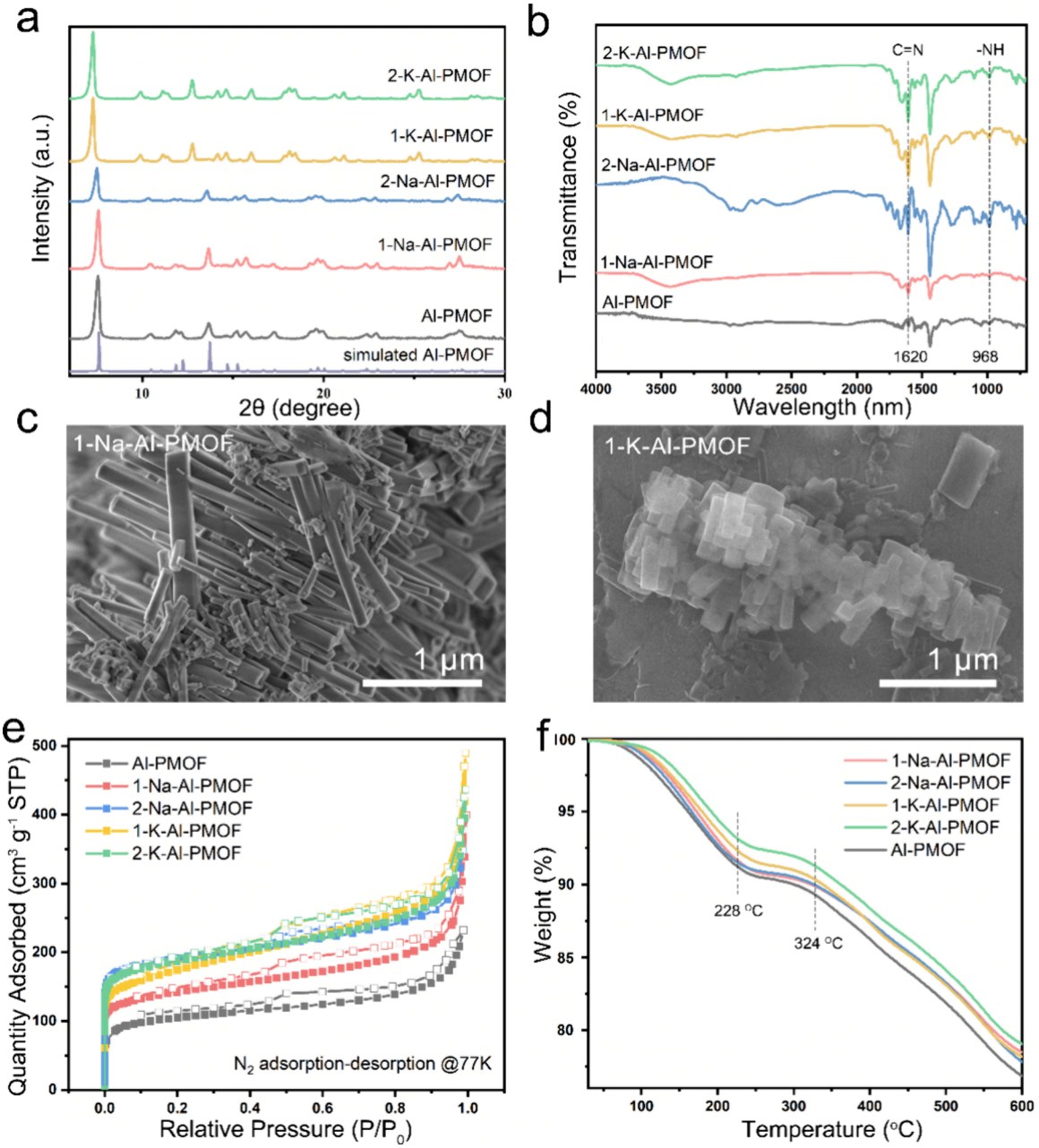

Figure 1. (a) XRD patterns of Al-PMOF and M-Al-PMOF (M = Na, K). SEM images of (b) 1-Na-Al-PMOF and (c) 1-K-Al-PMOF. (d) FTIR spectra of Al-PMOF and M-Al-PMOFs in the range of 3500−600 cm^{-1}. (e) N_2 adsorption and desorption isotherms of Al-PMOF and M-Al-PMOFs (solid point, adsorption; hollow point, desorption). (f) Thermogravimetric curve of Al-PMOF and M-Al-PMOFs.

https://doi.org/10.1021/acsaenm.5c00076
ACS Appl. Eng. Mater. XXXX, XXX, XXX−XXX

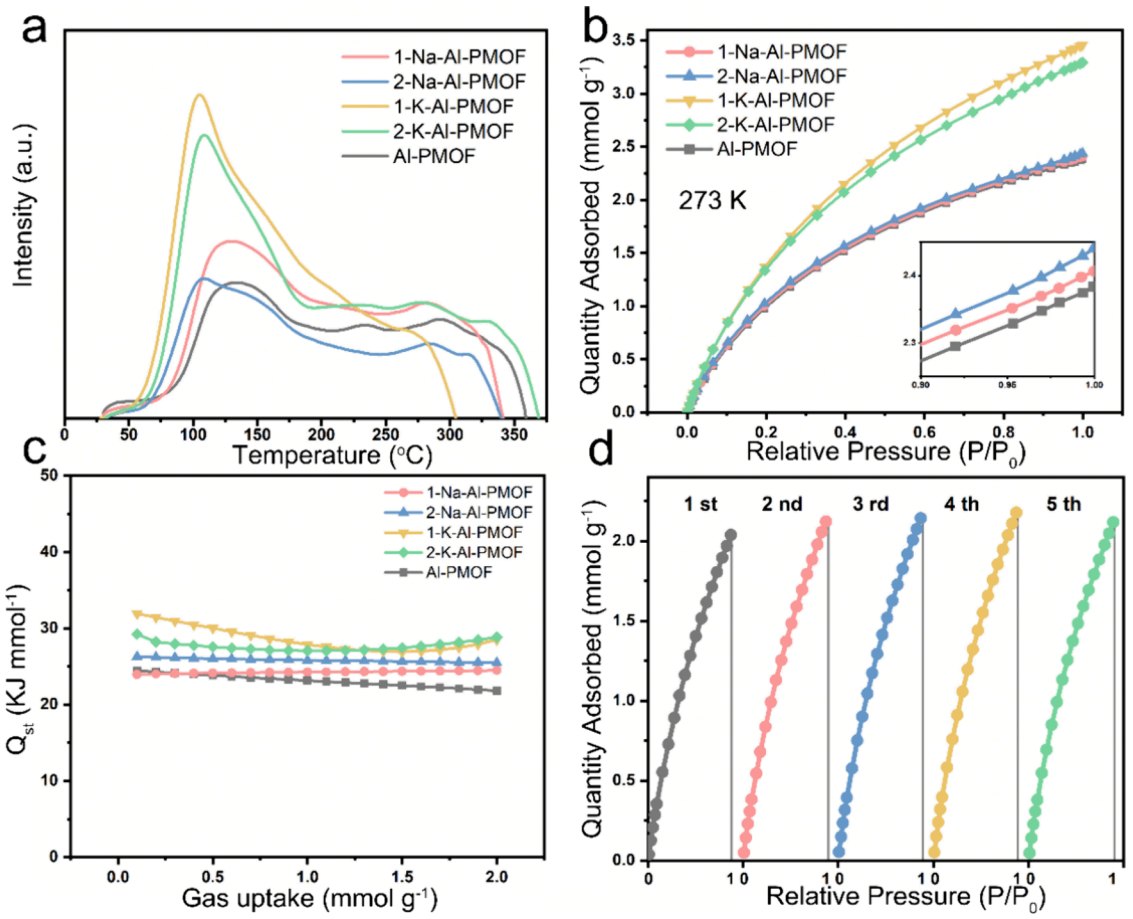

Figure 2. (a) CO_2-TPD curves of Al-PMOF and M-Al-PMOF (M = Na, K). (b) Static CO_2 adsorption curve of the samples at 273.15 K. (c) Isosteric heat of adsorption as a function of CO_2 uptake derived by the virial equation. (d) Five consecutive cycles of CO_2 adsorption with 1-K-Al-PMOF.

were less than 0.02 eV $Å^{-1}$. The VESTA software package was employed to visualize the electronic structure of the photocatalysts.[22]

The calculations of Gibbs free energy changes (ΔG) of absorption energy were performed according to the following eq 2:

$$\Delta G = \Delta E + \Delta \mathrm{ZPE} - T\Delta S \quad (2)$$

where E, ZPE, and S represent the total energy of the optimized system, zero-point energy, and entropy of species, respectively, and T denotes the temperature in Kelvin (set to be 298.15 K).

3. RESULTS AND DISCUSSION

We report an in situ doping hydrothermal strategy to synthesize M-Al-PMOF (M = Na, K), as illustrated in Scheme 1. The original Al-PMOF was synthesized by a hydrothermal method using the ligand H_2TCPP and Al salt as precursors. The digital photographs of all composite powder samples are provided in Figure S2. The powders appeared as dark green as observed by the naked eye; however, it is difficult to display in digital images. According to the different amounts of doped alkali metals, we prepared Al-PMOF, 1-Na-Al-PMOF, 2-Na-Al-PMOF, 1-K-Al-PMOF, and 2-K-Al-PMOF samples, respectively. In particular, Al-PMOF with 0.25 mmol of NaCl was denoted as 1-Na-Al-PMOF, and Al-PMOF with 0.5 mmol of NaCl was denoted as 2-Na-Al-PMOF. Similarly, Al-PMOF with 0.25 mmol of KCl was denoted as 1-K-Al-PMOF, and Al-PMOF with 0.5 mmol of KCl was denoted as 2-K-Al-PMOF.

3.1. Material Characterization

As shown in Figure 1a, the XRD analysis demonstrates the excellent crystallinity and purity of all samples, further confirming the successful synthesis and preparation of Al-PMOF and M-Al-PMOFs. It shows that after doping of alkali metals, the framework remained the same as pristine Al-PMOF. However, close inspection (Figure S3) shows that, compared with 1-Na-Al-PMOF, the diffraction peak of 2-Na-Al-PMOF shifted to a smaller angle, which indicates that an increased amount of doping cations led to an expansion of the lattice constant.[23] Similarly, when K^+ cations were doped instead of Na^+, the diffraction peak showed a shift to a smaller angle, indicating that doping with larger cations resulted in an increase in the lattice constant of MOFs. FTIR spectroscopy (Figure 1b) was conducted to characterize the molecular structure of the samples. The unique C═N stretching vibration of the porphyrin appeared at 1620 cm^{-1}.[24] The stretching −NH absorption peaks at 968 cm^{-1} in all samples indicate that no metal ion has coordinated with the −NH inside the porphyrin ring.[25] The SEM images (Figures 1c,d and S4) displayed the morphology of all samples. Both Na-doped and K-doped Al-PMOF were rod-like crystals similar to Al-PMOF. However, after doping with different cations, the crystal diameter of the K-doped samples was larger than that of the Na-doped material, which was consistent with our XRD results. The concentration of the Al atom and doped Na and K

https://doi.org/10.1021/acsaenm.5c00076
ACS Appl. Eng. Mater. XXXX, XXX, XXX−XXX

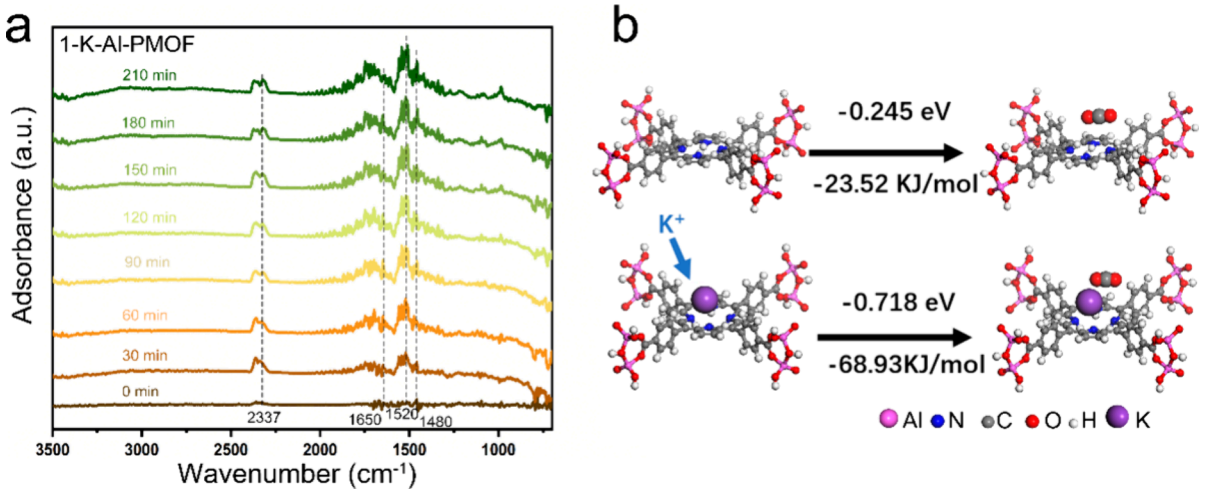

Figure 3. (a) In situ FTIR spectra of 1-K-Al-PMOF with continuous CO_2 gas filling. (b) CO_2 adsorption energy on Al-PMOF and 1-K-Al-PMOF calculated by VASP.

atoms was conducted by ICP-OES (Table S1), confirming the successful incorporation of different amounts of alkali metals.

The BET surface area (Figure 1e and Table S2) of Al-PMOF and M-Al-PMOF was conducted under N_2 adsorption at 77K. At lower pressure, the adsorption of N_2 increases sharply, indicating that the structures of these samples contain a large number of micropores.[26] The specific surface area of Al-PMOF is 398.5 $m^2\ g^{-1}$, which is consistent with the previous literature.[16] The results indicated that upon incorporation of alkali metals, K-Al-PMOFs had a larger surface specific area than Na-Al-PMOFs. Increased doping amounts resulted in larger surface specific areas, which aligned with similar research from Zhang et al.[27] Notably, 2-K-Al-PMOF exhibits the largest specific surface area, reaching 704.4 $m^2\ g^{-1}$, which surpasses the original Al-PMOF by 1.77 times. Moreover, the microporous volumes (M_v) of M-Al-PMOF are also larger than those of Al-PMOF, indicating more pores and channels for gas absorption. The thermal stability curve of the sample (Figure 1f) was conducted by TGA. The TGA curves exhibit two remarkable weight loss regions due to the removal of solvents below 228 °C and the collapse of structures above 324 °C. Within the temperature range of 228−324 °C, the samples retained stability and structural integrity. Also, the order of thermal stability of the samples is 2-K-Al-PMOF > 1-K-Al-PMOF > 2-Na-Al-PMOF > 1-Na-Al-PMOF > Al-PMOF, indicating that doping of alkali metals enhanced the thermal stability of the samples.

3.2. CO_2 Adsorption Properties

CO_2-TPD (Figure 2a) tests were first conducted to evaluate the CO_2 adsorption capacity of the samples. All samples exhibited weak physical adsorption around 110 °C and chemical desorption signals in the temperature range of 250−400 °C.[28] After doping modification, the amount of alkaline sites of the sample increased, which was more conducive to the adsorption of CO_2 (as a Lewis acid gas). Furthermore, K-Al-PMOFs showed the highest peak intensity at 110 °C in CO_2-TPD, indicating more alkaline sites than Na-doped samples and the original Al-PMOF. Masala et al.[29] and Cui et al.[13] also proved that K^+ had a strong interaction with CO_2, and the configuration of $K^+\cdots O{=}C{=}O$ facilitated the activation of CO_2.

The CO_2 capture performance was then evaluated by static adsorption tests. The CO_2 adsorption isotherms at 273.15 K (Figure 2b) showed that the static CO_2 adsorption capacity of Al-PMOF was 2.38 mmol g^{-1}, aligning with the previous research.[30] The CO_2 adsorption capacities of 2-K-Al-PMOF, 1-K-Al-PMOF, 2-Na-Al-PMOF, and 1-Na-Al-PMOF were 3.29, 3.46, 2.44, and 2.40 mmol g^{-1}, respectively, representing increases of 38.23, 45.38, 2.52, and 0.84% compared to that of Al-PMOF (Table S3). The increase in the CO_2 absorption capacity verified that the doping of alkali metals enhanced the adsorption capacity of the materials, and K doping exhibited better CO_2 adsorption performance as expected. With the CO_2 adsorption isotherms at 298.15 K (Figure S5), the isosteric heat of adsorption (Q_{st}) was calculated through a virial equation.[31] 1-K-Al-PMOF exhibited the highest Q_{st} values of CO_2 (31.9 kJ mol^{-1}) at zero loading, followed by 2-K-Al-PMOF (29.2 kJ mol^{-1}), 2-Na-Al-PMOF (26.3 kJ mol^{-1}), 1-Na-Al-PMOF (23.9 kJ mol^{-1}), and Al-PMOF (24.4 kJ mol^{-1}) (Figure 2c). A higher Q_{st} value signifies a stronger interaction between gas molecules and adsorbents, reflecting the increased affinity of the adsorption sites.[32] The Q_{st} value aligned with the CO_2 adsorption capacities of the samples further confirms that the incorporation of alkali metals enhanced the CO_2 absorption performance. Compared with other modified Al-MOFs (Table S4), alkali-metal-doped Al-MOFs show superior CO_2 adsorption performance. Furthermore, when compared with existing MOFs reported in the literature, our K-doped Al-PMOFs also exhibit good CO_2 capture capabilities. Moreover, Figure 2d shows the results of five cycles of CO_2 adsorption isotherm tests for 1-K-Al-PMOF. Before each test, the material was pretreated in a vacuum at 120 °C and then subjected to the CO_2 adsorption test at 273.15 K. After five cycles of tests, no hysteresis or performance degradation was observed, demonstrating its stability, recyclability, and application value. However, the adsorption properties of the materials in multicomponent gases need to be explored further. In practical application, the gas mixture may contain various components like N_2 and H_2O, and the CO_2 adsorption capacity of the materials in such mixed gases needs to be assessed.

To better understand the CO_2 adsorption mechanism at the molecular level, time-resolved in situ FTIR spectroscopy was conducted to further determine the adsorbed species formed upon CO_2 uptake. The in situ FTIR spectra of M-Al-PMOF in

https://doi.org/10.1021/acsaenm.5c00076
ACS Appl. Eng. Mater. XXXX, XXX, XXX−XXX

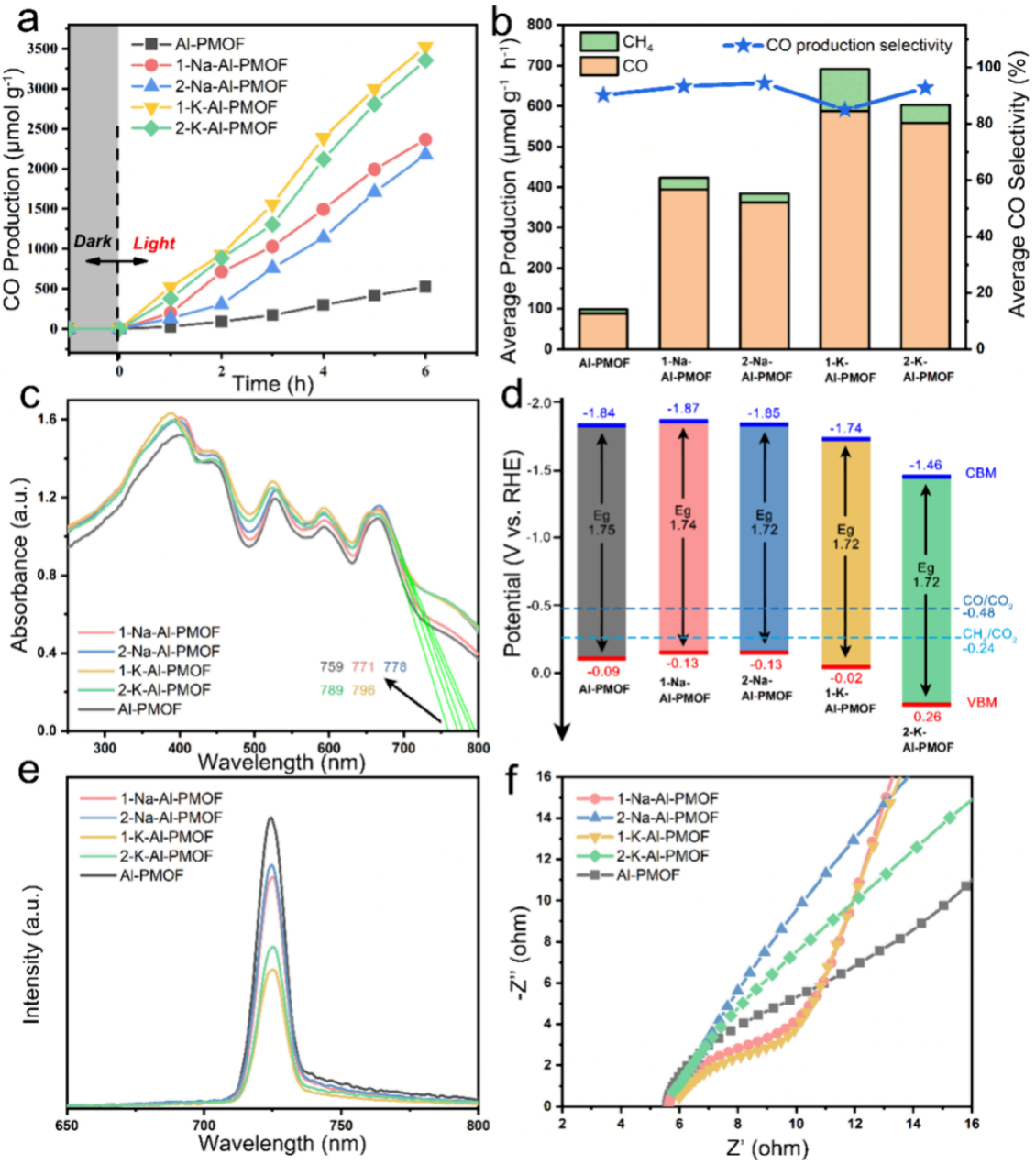

Figure 4. (a) Time-dependent CO production upon xenon lamp irradiation and (b) production rates and selectivity for Al-PMOF and M-Al-PMOF (M = Na, K). (c) UV−vis diffuse reflectance spectra and (d) schematic diagram of the band structure for Al-PMOF and M-Al-PMOF. (e) PL and (f) EIS spectra of Al-PMOF and M-Al-PMOF.

CO_2 under ambient pressure at room temperature were recorded as a function of time (Figures 3a and S6). The newly formed absorption peaks observed after the introduction of CO_2 indicate the adsorbed species on the adsorbent. The vibration at 2337 cm^{-1} corresponds to physically adsorbed CO_2 via van der Waals interactions, which is different from the free gas-phase CO_2.[33] The peaks at 1650, 1520, and 1480 cm^{-1} are assigned to the surface-adsorbed carbonate species, including monodentate carbonate (m-CO_3^{2-}) and bidentate carbonate (b-CO_3^{2-}), where m-CO_3^{2-} binds through one oxygen atom to the metal site, while b-CO_3^{2-} bridges two adjacent metal sites.[34−36] The FTIR results strongly indicate that the physically adsorbed CO_2 and the formation of carbonate species may contribute to the massive metal sites, porphyrin skeleton, and amine groups in the framework. Also, we calculated the adsorption energy of a single CO_2 molecule adsorbed in the MOF structure through VASP.[37] As shown in Figure 3b, the incorporation of a single alkali metal ion increased the adsorption energy by 0.473 eV. The calculated and experimental results both showed that doping alkali metals could effectively enhance the CO_2 adsorption capacity of the materials.

3.3. Photoelectric Performance and Photocatalytic CO_2 Reduction Performance

The photocatalytic CO_2 reduction reaction (CORR) performance of M-Al-PMOF (M = Na, K) was examined in a CO_2-saturated solution under xenon lamp irradiation. As shown in Figures 4a, b and S7, no gases are produced in a dark environment. Under continuous xenon lamp illumination, CO and CH_4 are produced by photocatalytic CORR, and the

https://doi.org/10.1021/acsaenm.5c00076
ACS Appl. Eng. Mater. XXXX, XXX, XXX−XXX

production amounts of both CO and CH_4 increase linearly over time. Al-PMOF has an average CO yield of 88.3 μmol g^{-1} $h^{-1}_{cat.}$ and an average CH_4 yield of 9.68 μmol g^{-1} $h^{-1}_{cat.}$ over 6 h; hence, the selectivity of CO is calculated to be 90.1%. With the same test conditions, all alkali-metal-doped Al-PMOFs exhibit superior CO yields. Notably, 1-K-Al-PMOF achieved the highest CO yield of 587.2 μmol g^{-1} $h^{-1}_{cat.}$, which is 6.6 times of the CO yield obtained by using Al-PMOF. Moreover, the CO yields of 2-K-Al-PMOF, 1-Na-Al-PMOF, and 2-Na-Al-PMOF are 558.9, 394.4, and 362.3 μmol g^{-1} $h^{-1}_{cat.}$, respectively, and their selectivity of CO is higher than 90%. The experimental results reveal that K-doped Al-PMOFs exhibit superior photocatalytic CORR performance compared with Na-doped Al-PMOFs. This improvement is likely attributed to a synergistic effect, whereby K^+ ions not only enhance CO_2 adsorption capacity but also actively promote the reduction kinetics. The observed trend aligns with the electrocatalytic CORR mechanism reported by Gu et al.,[38] where K^+ ions interact with the electric field and the dipole moment of the adsorptive intermediate. Our study extends this understanding to photocatalytic processes, demonstrating that among various alkali metals, K-doped Al-PMOFs exhibit the best catalytic performance. Control experiments were conducted to confirm that CO and CH_4 were produced from CO_2 as the carbon source (Table S5). In addition, the CO_2 adsorption capacity, light source, and catalytic reduction to CO production were compared with other references (Table S6). Compared with the photocatalysts previously reported in the literature, this work achieves the efficient photocatalytic conversion of CO_2 to CO. Furthermore, although the catalyst exhibits stable performance over the 6 h test period, industrial applications demand prolonged operation under cyclic conditions. Accelerated aging tests (e.g., 500 h continuous illumination) will be conducted to assess durability in the future.

To gain insight into the role of alkali metals in enhancing photocatalytic activity, we investigated the photoelectric performance of our photocatalysts. UV−vis diffuse reflectance spectroscopy (Figure 4c) shows that all Al-PMOFs exhibit an absorption edge reaching 760 nm, enabling efficient utilization of visible-near-infrared light. This broad light-harvesting range is critical for maximizing solar energy utilization in photocatalytic CO_2 reduction. Meanwhile, the absorption is slightly enhanced after doping with alkali metals. The band gaps (E_g) of all samples are calculated based on the Tauc plots from the transformed Kubelka−Munk function (Figure S8), and the flat band potentials of all samples are obtained by Mott−Schottky plots (Figure S9). Then, the band structures of all samples were outlined in Figure 4d. Notably, the conduction band minima (CBM) of all samples exhibit sufficient negativity in comparison to the reduction potentials of CO/CO_2 (−0.48 V vs RHE) and CH_4/CO_2 (−0.24 V vs RHE), indicating the thermodynamic feasibility of photocatalytic CORR. The steady-state PL spectroscopy results (Figure 4e) of all samples show that alkali-metal-doped samples exhibit significantly lower PL intensity compared to pristine Al-PMOF, indicating effective suppression of the photogenerated charge carrier recombination with alkali metal incorporation. This quenching of recombination directly enhances the photocatalytic performance by preserving more charge carriers for catalytic reactions. As shown in Figure 4f, the Nyquist plots of 1-K-Al-PMOF and 1-Na-Al-PMOF display similar radii, suggesting comparable and relatively lower interfacial charge transfer resistance (R_{ct}). Additionally, the observed Warburg impedance (Z_w) in these samples corresponds to the CO_2 mass transport resistance during the catalytic process. However, 1-K-Al-PMOF and 1-Na-PMOF exhibit better catalytic performance than 2-K-Al-PMOF and 2-Na-Al-PMOF, respectively, indicating that the doping concentration of alkali metals influences catalytic efficiency by modulating interfacial charge transfer dynamics. These findings align with the PL results that lower alkali metal doping levels preserve a higher population of photogenerated charge carriers available for CO_2 reduction, thereby optimizing the photocatalytic activity. However, in TPR spectra (Figure S10), the photocurrent density of alkali-metal-doped Al-PMOFs was lower than that of Al-PMOF under light irradiation, which means that the charge generation efficiency was inhibited by alkali metal doping. The above photoelectric test results show that the introduction of alkali metals effectively reduces the band gap and suppresses the recombination of charge carriers; however, it can inhibit charge generation efficiency. Our mechanistic analysis suggests that the enhanced photocatalytic CORR activity in alkali-metal-doped Al-PMOFs is primarily attributed to a dual-function mechanism combining optimized CO_2 chemisorption capacity and alkali-cation-mediated catalytic promotion, rather than significant alterations in the material's intrinsic photoelectronic characteristics. Also, the specific electron transfer process and the formation of intermediates during the CO_2 catalytic reduction process require further exploration through in situ characterization and computational methods.

4. CONCLUSIONS

In this study, we successfully synthesized M-Al-PMOFs (M = Na and K) by introducing alkali metals Na and K to modify the Al-PMOF, and their CO_2 capture and photocatalytic properties were investigated. These alkali-metal-doped MOFs exhibited improved CO_2 adsorption capacity due to their increased surface area and amount of alkaline sites, up to 40% higher than Al-PMOF. Comprehensive experiments showed that the photocatalytic CORR performance of alkali-metal-doped MOFs was improved, especially the yield of CO by 1-K-Al-PMOF is 6.6 times higher than that of Al-PMOF. In addition, we found that K-doped MOFs showed better absorption capacity and photocatalytic CORR performance than Na-doped MOFs. Our work provides an effective strategy for doping alkali metals in MOFs to improve their CO_2 adsorption performance while enhancing their photocatalytic CORR performance.

■ ASSOCIATED CONTENT

Supporting Information

The Supporting Information is available free of charge at https://pubs.acs.org/doi/10.1021/acsaenm.5c00076.

Diagram of the photocatalytic reactor (Figure S1); digital photographs of all the composite powders (Figure S2); XRD patterns of the samples (Figure S3); SEM images of the samples (Figure S4); static CO_2 adsorption curve of the samples at 298 K (Figure S5); in situ FTIR spectra of Al-PMOF and 1-Na-Al-PMOF with continuous CO_2 gas filling (Figure S6); time-dependent CH_4 production of the samples (Figure S7); estimated band gaps of the samples (Figure S8); Mott−Schottky plot of the samples (Figure S9); transient photocurrent response spectra of the samples (Figure

https://doi.org/10.1021/acsaenm.5c00076
ACS Appl. Eng. Mater. XXXX, XXX, XXX−XXX

S10); concentration of elements in ICP-OES experiments (Table S1); structural parameters of samples (Table S2); CO_2 adsorption properties of samples (Table S3); comparison of CO_2 adsorption properties with other MOFs (Table S4); photocatalytic CO_2 reduction control experiment (Table S5); and comparison of the photocatalytic CO_2 reduction activities of recently reported catalysts (Table S6) (PDF)

AUTHOR INFORMATION

Corresponding Author

Jing Sun − *State Key Lab of High Performance Ceramics and Superfine Microstructure, Shanghai Institute of Ceramics, Chinese Academy of Sciences, Shanghai 201899, China;* orcid.org/0000-0003-1101-1584; Phone: +86-021-69163785; Email: jingsun@mail.sic.ac.cn

Authors

Chenyue Yong − *State Key Lab of High Performance Ceramics and Superfine Microstructure, Shanghai Institute of Ceramics, Chinese Academy of Sciences, Shanghai 201899, China; University of Chinese Academy of Sciences, Beijing 100049, China;* orcid.org/0009-0006-1610-9299

Guanhong Lu − *State Key Lab of High Performance Ceramics and Superfine Microstructure, Shanghai Institute of Ceramics, Chinese Academy of Sciences, Shanghai 201899, China*

Xiao Wang − *State Key Lab of High Performance Ceramics and Superfine Microstructure, Shanghai Institute of Ceramics, Chinese Academy of Sciences, Shanghai 201899, China;* orcid.org/0000-0001-9786-8153

Gansheng Shi − *State Key Lab of High Performance Ceramics and Superfine Microstructure, Shanghai Institute of Ceramics, Chinese Academy of Sciences, Shanghai 201899, China*

Yan Wang − *State Key Lab of High Performance Ceramics and Superfine Microstructure, Shanghai Institute of Ceramics, Chinese Academy of Sciences, Shanghai 201899, China;* orcid.org/0000-0002-0971-5032

Xiaofeng Xie − *State Key Lab of High Performance Ceramics and Superfine Microstructure, Shanghai Institute of Ceramics, Chinese Academy of Sciences, Shanghai 201899, China;* orcid.org/0000-0003-1789-1084

Complete contact information is available at: https://pubs.acs.org/10.1021/acsaenm.5c00076

Author Contributions

C.Y. was responsible for executing the experiments, preparing the samples, evaluating the properties, and drafting the manuscript. G.L., G.S., Y.W., and X.X. provided valuable comments. J.S. supervised this project and revised the manuscript. All authors have concurred and approved the definitive version of this manuscript.

Notes

The authors declare no competing financial interest.

ACKNOWLEDGMENTS

This work was financially supported by the Shanghai Commission of Science and Technology Program (CXXT-2023-01) and the National Natural Science Foundation of China (52072387).

REFERENCES

(1) He, H. Z.; Kramer, R. J.; Soden, B. J.; Jeevanjee, N. State Dependence of CO_2 Forcing and its Implications for Climate Sensitivity. *Science* **2023**, *382* (6674), 1051−1056.

(2) Filonchyk, M.; Peterson, M. P.; Yan, H.; Gusev, A.; Zhang, L.; He, Y.; Yang, S. Greenhouse Gas Emissions and Reduction Strategies for the World's Largest Greenhouse Gas Emitters. *Sci. Total Environ.* **2024**, *944*, No. 173895.

(3) Zhang, W.; Deng, C.; Wang, W.; Sheng, H.; Zhao, J. Achieving Almost 100% Selectivity in Photocatalytic CO_2 Reduction to Methane via In-Situ Atmosphere Regulation Strategy. *Adv. Mater.* **2024**, *36* (35), No. 2405825.

(4) Sadanandan, A. M.; Yang, J.-H.; Devtade, V.; Singh, G.; Panangattu Dharmarajan, N.; Fawaz, M.; Mee Lee, J.; Tavakkoli, E.; Jeon, C.-H.; Kumar, P.; Vinu, A. Carbon Nitride Based Nanoarchitectonics for Nature-Inspired Photocatalytic CO_2 Reduction. *Prog. Mater. Sci.* **2024**, *142*, No. 101242.

(5) Sun, H.; Sun, S.; Liu, T.; Zeng, J.; Wang, Y.; Yan, Z.; Wu, C. Integrated CO_2 Capture and Utilization: Selection, Matching, and Interactions between Adsorption and Catalytic Sites. *ACS Catal.* **2024**, *14* (20), 15572−15589.

(6) Kong, F.; Chen, W. Carbon Dioxide Capture and Conversion Using Metal−Organic Framework (MOF) Materials: A Comprehensive Review. *Nanomaterials* **2024**, *14* (16), 1340.

(7) Mandal, S.; Natarajan, S.; Mani, P.; Pankajakshan, A. Post-Synthetic Modification of Metal−Organic Grameworks Toward Applications. *Adv. Funct. Mater.* **2021**, *31* (4), No. 2006291.

(8) Masoomi, M. Y.; Morsali, A.; Dhakshinamoorthy, A.; Garcia, H. Mixed-Metal MOFs: Unique Opportunities in Metal−Organic Framework (MOF) Functionality and Design. *Angew. Chem., Int. Ed.* **2019**, *58* (43), 15188−15205.

(9) He, T.; Cao, H.; Chen, P. The Roles of Alkali/Alkaline Earth Metals in the Materials Design and Development for Hydrogen Storage. *Acc. Mater. Res.* **2021**, *2* (9), 726−738.

(10) Yeganegi, S.; Sokhanvaran, V. Adsorption of Hydrogen and Methane on Intrinsic and Alkali Metal Cations-Doped $Zn_2(NDC)_2(diPyTz)$ Metal−Organic Framework Using GCMC Simulations. *Adsorption* **2016**, *22* (2), 277−285.

(11) Karikkethu Prabhakaran, P.; Deschamps, J. Hydrogen Adsorption in Lithium Doped MIL-101 and MIL-53(Al) at 77 and 298 K Up to 100 bar: Effect of Lithium Concentration. *J. Porous Mater.* **2015**, *22* (4), 1073−1081.

(12) Akbari Beni, F.; Niknam Shahrak, M. Alkali Metals-Promoted Capacity of ZIF-8 and ZIF-90 for Carbon Capturing: A Molecular Simulation Study. *Polyhedron* **2020**, *178*, No. 114338.

(13) Cui, S.; Gu, Y.; Shao, Y.; Zhong, W. Experimental Research of Alkali Metals Modified Mg/DOBDC Metal Organic Framework as High Capacity CO_2 Adsorbent. *Sep. Purif. Technol.* **2024**, *331*, No. 125471.

(14) Boyd, P. G.; Chidambaram, A.; Garcia-Diez, E.; Ireland, C. P.; Daff, T. D.; Bounds, R.; Gladysiak, A.; Schouwink, P.; Moosavi, S. M.; Maroto-Valer, M. M.; Reimer, J. A.; Navarro, J. A. R.; Woo, T. K.; Garcia, S.; Stylianou, K. C.; Smit, B. Data-Driven Design of Metal-Organic Frameworks for Wet Flue Gas CO_2 Capture. *Nature* **2019**, *576* (7786), 253−256.

(15) Wang, K.; Liu, Y.; Kang, J.; Zhang, Y.; Wang, Q.; Chen, L.; Wang, Q.; Liu, B.; Liu, M.; Qiu, X.; Li, W.; Li, J. Site-Selective Photocoupled Electrocatalytic CO_2 Reduction over Efficient Al-oxo Chain Based-Porphyrin Framework. *Appl. Catal., B* **2023**, *325*, No. 122315.

(16) Shang, S. S.; Xiong, W.; Yang, C.; Johannessen, B.; Liu, R. G.; Hsu, H. Y.; Gu, Q. F.; Leung, M. K. H.; Shang, J. Atomically Dispersed Iron Metal Site in a Porphyrin-Based Metal-Organic Framework for Photocatalytic Nitrogen Fixation. *ACS Nano* **2021**, *15* (6), 9670−9678.

(17) Fateeva, A.; Chater, P. A.; Ireland, C. P.; Tahir, A. A.; Khimyak, Y. Z.; Wiper, P. V.; Darwent, J. R.; Rosseinsky, M. J. A Water-Stable Porphyrin-Based Metal−Organic Framework Active for Visible-Light Photocatalysis. *Angew. Chem., Int. Ed.* **2012**, *51* (30), 7440−7444.

(18) Li, X.; Li, L.; Chen, G.; Chu, X.; Liu, X.; Naisa, C.; Pohl, D.; Löffler, M.; Feng, X. Accessing Parity-Forbidden D-D Transitions for Photocatalytic CO_2 Reduction Driven by Infrared Light. *Nat. Commun.* **2023**, *14* (1), 4034.
(19) Kresse, G.; Furthmüller, J. Efficiency of Ab-Initio Total Energy Calculations for Metals and Semiconductors Using a Plane-Wave Basis Set. *Comput. Mater. Sci.* **1996**, *6* (1), 15−50.
(20) Perdew, J. P.; Burke, K.; Ernzerhof, M. Generalized Gradient Approximation Made Simple. *Phys. Rev. Lett.* **1996**, *77* (18), 3865−3868.
(21) Grimme, S.; Antony, J.; Ehrlich, S.; Krieg, H. A Consistent and Accurate Ab Initio Parametrization of Density Functional Dispersion Correction (DFT-D) for the 94 Elements H-Pu. *J. Chem. Phys.* **2010**, *132* (15), 154104.
(22) Momma, K.; Izumi, F. VESTA 3 for Three-Dimensional Visualization of Crystal, Volumetric and Morphology Data. *J. Appl. Crystallogr.* **2011**, *44*, 1272−1276.
(23) Wang, X.; Tuo, Y.; Zhou, Y.; Wang, D.; Wang, S.; Zhang, J. Ta-Doping Triggered Electronic Structural Engineering and Strain Effect in NiFe LDH for Enhanced Water Oxidation. *Chem. Eng. J.* **2021**, *403*, No. 126297.
(24) Zhen, W.; Kang, D. W.; Fan, Y.; Wang, Z.; Germanas, T.; Nash, G. T.; Shen, Q.; Leech, R.; Li, J.; Engel, G. S.; Weichselbaum, R. R.; Lin, W. Simultaneous Protonation and Metalation of a Porphyrin Covalent Organic Framework Enhance Photodynamic Therapy. *J. Am. Chem. Soc.* **2024**, *146* (24), 16609−16618.
(25) Wen, B.; Huang, Y.; Jiang, Z.; Wang, Y.; Hua, W.; Indris, S.; Li, F. Exciton Dissociation into Charge Carriers in Porphyrinic Metal-Organic Frameworks for Light-Assisted Li-O_2 Batteries. *Adv. Mater.* **2024**, *36* (32), No. 2405440.
(26) Song, L.; Zhang, X.; Chen, C.; Liu, X.; Zhang, N. UTSA-16 as an Efficient Microporous Catalyst for CO_2 Conversion to Cyclic Carbonates. *Microporous Mesoporous Mater.* **2017**, *241*, 36−42.
(27) Zhang, X.; Chen, Z.; Yang, X.; Li, M.; Chen, C.; Zhang, N. The Fixation of Carbon Dioxide with Epoxides Catalyzed by Cation-Exchanged Metal-Organic Framework. *Microporous Mesoporous Mater.* **2018**, *258*, 55−61.
(28) Wang, Z.; Zhou, W.; Wang, X.; Zhang, X.; Chen, H.; Hu, H.; Liu, L.; Ye, J.; Wang, D. Enhanced Photocatalytic CO_2 Reduction over TiO_2 Using Metalloporphyrin as the Cocatalyst. *Catalysts* **2020**, *10*, 654.
(29) Masala, A.; Vitillo, J. G.; Bonino, F.; Manzoli, M.; Grande, C. A.; Bordiga, S. New Insights into UTSA-16. *Phys. Chem. Chem. Phys.* **2016**, *18* (1), 220−227.
(30) Shang, S.; Yang, C.; Sun, M.; Tao, Z.; Hanif, A.; Gu, Q.; Shang, J. CO_2 Capture from Wet Flue Gas Using Transition Metal Inserted Porphyrin-Based Metal-Organic Frameworks as Efficient Adsorbents. *Sep. Purif. Technol.* **2022**, *301*, No. 122058.
(31) Dong, B. X.; Zhang, S. Y.; Liu, W. L.; Wu, Y. C.; Ge, J.; Song, L.; Teng, Y. L. Gas Storage and Separation in a Water-Stable $[CuI_5BTT_3]^{4-}$ Anion Framework Comprising a Giant Multi-Prismatic Nanoscale Cage. *Chem. Commun. (Cambridge, U. K.)* **2015**, *51* (26), 5691−5694.
(32) Sumida, K.; Rogow, D. L.; Mason, J. A.; McDonald, T. M.; Bloch, E. D.; Herm, Z. R.; Bae, T.-H.; Long, J. R. Carbon Dioxide Capture in Metal−Organic Frameworks. *Chem. Rev.* **2012**, *112* (2), 724−781.
(33) Mihaylov, M.; Chakarova, K.; Andonova, S.; Drenchev, N.; Ivanova, E.; Sabetghadam, A.; Seoane, B.; Gascon, J.; Kapteijn, F.; Hadjiivanov, K. Adsorption Forms of CO_2 on MIL-53(Al) and NH_2-MIL-53(Al) as Revealed by FTIR Spectroscopy. *J. Phys. Chem. C* **2016**, *120* (41), 23584−23595.
(34) Wang, X.; Schwartz, V.; Clark, J. C.; Ma, X.; Overbury, S. H.; Xu, X.; Song, C. Infrared Study of CO_2 Sorption over "Molecular Basket" Sorbent Consisting of Polyethylenimine-Modified Mesoporous Molecular Sieve. *J. Phys. Chem. C* **2009**, *113* (17), 7260−7268.
(35) Lavalley, J. C. Infrared Spectrometric Studies of the Surface Basicity of Metal Oxides and Zeolites Using Adsorbed Probe Molecules. *Catal. Today* **1996**, *27* (3), 377−401.
(36) Ma, Y.; Yi, X.; Wang, S.; Li, T.; Tan, B.; Chen, C.; Majima, T.; Waclawik, E. R.; Zhu, H.; Wang, J. Selective Photocatalytic CO_2 Reduction in Aerobic Environment by Microporous Pd-Porphyrin-Based Polymers Coated Hollow TiO_2. *Nat. Commun.* **2022**, *13* (1), 1400.
(37) Mu, W.; Liu, D.; Zhong, C. A Computational Study of the Effect of Doping Metals on CO_2/CH_4 Separation in Metal−Organic Frameworks. *Microporous Mesoporous Mater.* **2011**, *143* (1), 66−72.
(38) Gu, J.; Liu, S.; Ni, W.; Ren, W.; Haussener, S.; Hu, X. Modulating Electric Field Distribution by Alkali Cations for CO_2 Electroreduction in Strongly Acidic Medium. *Nature Catalysis* **2022**, *5* (4), 268−276.

https://doi.org/10.1021/acsaenm.5c00076
ACS Appl. Eng. Mater. XXXX, XXX, XXX−XXX